

# X-ray Spectromicroscopy Study of Protein Adsorption to a Polystyrene–Polylactide Blend

Bonnie O. Leung,<sup>\*†</sup> Adam P. Hitchcock,<sup>†</sup> Rena Cornelius,<sup>‡</sup> John L. Brash,<sup>‡</sup>  
Andreas Scholl,<sup>§</sup> and Andrew Doran<sup>§</sup>

BIMR and School of Biomedical Engineering, McMaster University, Hamilton, Ontario, Canada L8S 4M1,  
and Advanced Light Source, Berkeley Lab, Berkeley, California 94720

Received March 3, 2009; Revised Manuscript Received May 8, 2009

Synchrotron-based X-ray photoemission electron microscopy (X-PEEM) was used to study the adsorption of human serum albumin (HSA) to polystyrene-polylactide (40:60 PS-PLA, 0.7 wt %) thin films, annealed under various conditions. The rugosity of the substrate varied from 35 to 90 nm, depending on the annealing conditions. However, the characteristics of the protein adsorption (amounts and phase preference) were not affected by the changes in topography. The adsorption was also not changed by the phase inversion which occurred when the PS-PLA substrate was annealed above  $T_g$  of the PLA. The amount of protein adsorbed depended on whether adsorption took place from distilled water or phosphate buffered saline solution. These differences are interpreted as a result of ionic strength induced changes in the protein conformation in solution.

## 1. Introduction

Polylactide (PLA), synthesized by ring-opening polymerization of lactide, is a biocompatible and biodegradable synthetic polyester commonly used in tissue engineering and as drug delivery vehicles. For scaffold engineering and drug microcapsules, the rate of degradation and controlled release, respectively, can be greatly impacted by combining a nonbiodegradable polymer such as polystyrene (PS)<sup>1</sup> or polyethylene glycol (PEG)<sup>2</sup> with a biodegradable material. The combination of biodegradable and nonbiodegradable polymers is known as a bioblend.<sup>3</sup> Bioblends can be a simple, cost-effective means of obtaining a composite with tunable physical or chemical properties.<sup>4</sup>

Protein adsorption to biomaterials is important for the biocompatibility of a material, because it is the first event that occurs after implantation of a medical device.<sup>5</sup> PLA is often blended with PEG to produce surface-PEGylated micelles capable of drug delivery.<sup>6–8</sup> Protein adsorption to these micro-particles shows a consistent trend of decreased adsorption with increased PEG at the surface.<sup>9,10</sup> Moreover, surface characterization of PLA-PEG spun cast films by X-ray photoelectron spectroscopy (XPS) reveals less protein adsorption compared to pure PLA.<sup>11</sup> However, a major limitation of these studies is the lack of information regarding the spatial distribution of the adsorbed protein relative to the individual components of the dual-polymer substrate.

We use soft X-ray spectromicroscopy techniques such as surface-sensitive synchrotron-based X-ray photoemission electron microscopy (X-PEEM) to visualize and quantitatively map biomolecules adsorbed to candidate biomaterials. Previously, our systematic X-PEEM studies of human serum albumin (HSA) or fibrinogen (Fg)<sup>12</sup> adsorption to phase-segregated PS-polymethyl methacrylate (PMMA) thin films with varying protein concentration,<sup>13</sup> exposure time, pH,<sup>14</sup> and protein-peptide

competitive adsorption<sup>15</sup> demonstrated that adsorption to PS-PMMA blend surfaces is controlled mainly by hydrophobic effects.

Recently, atomic force microscopy (AFM) and X-ray spectromicroscopy were used to characterize the morphology and phase segregation of a spun-cast PS-PLA bioblend.<sup>16</sup> It was found that the surface morphology depended on mass ratio, total polymer concentration, annealing time, and temperature. Phase segregation improved significantly when the film was heated above the glass transition temperature ( $T_g$ ) of PLA. This also resulted in a striking phase inversion where the discrete domains became PS-rich rather than PLA-rich.<sup>16</sup>

Here we report studies of the adsorption of HSA to this PS-PLA platform. In addition to investigating the effect of the phase inversion on protein adsorption, we examined the effect of topography since the rugosity of our polymer surface changed from a mean value of 35 to 90 nm rms upon annealing, while retaining similar chemical properties. Also, the effect of ionic strength was investigated by comparing the adsorption of HSA from distilled deionized (DDI) water and phosphate-buffered saline (PBS) solutions. This study is part of an ongoing effort to provide insight into the interaction of blood and blood components with phase-segregated and patterned polymer materials by mapping and quantifying the adsorption of the major blood proteins to candidate biomaterials. These results are intended to contribute to a better understanding of protein adsorption phenomena, which may lead to the development of tissue contacting medical devices of improved biocompatibility.

## 2. Materials and Methods

**2.1. Materials.** Polystyrene (MW = 104 K,  $\delta$  = 1.05) and polylactide (MW = 33 K,  $\delta$  = 1.33) were obtained from Polymer Source Inc. and used as received. PS/PLA 40:60, 0.7 wt % films were spun cast (4000 rpm, 40 s) from dichloromethane onto a clean 1 × 1 cm native oxide silicon wafer (Wafer World, Inc.), degreased with trichloroethylene, acetone, and methanol, followed by rinsing with DDI.

HSA was obtained from Behringwerke AG, Marburg, Germany, and found to be homogeneous as judged by sodium dodecyl sulfate polyacrylamide gel electrophoresis (SDS-PAGE). Protein solutions for

\* Corresponding author. E-mail: leungbo@mcmaster.ca.

† BIMR.

‡ School of Biomedical Engineering.

§ Advanced Light Source.

exposure were prepared with DDI water or PBS using HSA concentrations of 0.05, 0.01, and 0.005 mg/mL.

**2.2. Substrates and Protein Exposure.** Pure PS or PLA were dissolved in toluene or dichloromethane, respectively, and blends of PS with PLA (40:60 ratio) were dissolved in dichloromethane. The solutions were spun cast onto a cleaned native oxide silicon wafer. The PS/PLA substrates were annealed at 45 (1 h, 6 h) and 70 °C (1 h) in a vacuum oven at a pressure  $\sim 10^{-5}$  Torr, achieved with a cryo-trapped turbo pump. The morphology of these substrates and miscibility of the two components were previously characterized by atomic force microscopy (AFM) and X-ray spectromicroscopy.<sup>16</sup>

The films were annealed just prior to protein adsorption studies. The pure PS, pure PLA, or PS/PLA substrate was placed in a beaker, covered with 5 mL of 0.05, 0.01, or 0.005 mg/mL protein solution for 20 min and then diluted three times with at least 50 mL of DDI or PBS buffer. The substrate was removed and vigorously rinsed. The protein adsorbed sample was then carefully dried by touching the edge of the Si wafer with lens paper.

**2.3. Scanning Transmission X-ray Microscopy (STXM).** High quality near-edge X-ray absorption fine structure (NEXAFS) reference spectra of PS, PLA, and HSA were collected with STXM on beamline 5.3.2 at the Advanced Light Source (ALS) in Berkeley, CA, using X-rays with 80% linear polarization.<sup>17,18</sup> The STXM operates in transmission mode and offers slightly better energy resolution (0.1–0.2 eV) compared to X-PEEM (0.4–0.5 eV); however, similar NEXAFS line shapes are obtained from both methods. Typically, thin film samples with thickness below 100 nm are produced by solvent casting onto an X-ray transparent silicon nitride window. Micrometer size homogeneous areas were measured using image sequences<sup>19</sup> to minimize radiation damage. An image at a damage sensitive energy was recorded after each image sequence measurement to ensure negligible damage. All reference spectra were normalized so that the intensity scale of each component is set to the signal expected from 1 nm of the polymer or protein at its bulk density.

**2.4. X-PEEM.** All X-PEEM measurements were performed at ALS on bend magnet beamline 7.3.1 (PEEM-2). Detailed accounts of the experimental apparatus, beamline setup and instrument optics have been presented previously.<sup>20</sup> Briefly, photoelectrons and secondary electrons ejected by absorption of 70–80% right circularly polarized monochromatic X-rays are accelerated into an electrostatic imaging column, where the spatial distribution is magnified and detected by a CCD camera. Circularly polarized X-rays are used at PEEM-2 due to slightly better energy resolution compared to linear polarized X-rays. Thus the results are not affected by possible molecular alignment effects (linear dichroism). X-PEEM is a partial electron yield technique with a strong emphasis on low kinetic energy secondary electrons. Thus, X-PEEM is surface sensitive with a sampling depth ( $1/e$ ) of 4 nm for polymers<sup>21</sup> and an integrated sampling depth of the outer 10 nm of the sample.

With PEEM-2, a 100 nm thick titanium filter was used to eliminate second-order light. To reduce radiation damage, a shutter with a 0.1 s response time was implemented to block the X-ray beam during the time required to transfer images from the charge coupled device (CCD) camera and to step the photon energy. This resulted in an exposure reduction of 50%. The incident flux was reduced to about 10% of the full intensity by masking upstream of the monochromator, and a limited number of energies (23 in C 1s, 47 in N 1s) and a short exposure time per image (1 s) were used as other ways to minimize radiation damage. The field of view was approximately 20  $\mu\text{m}$ .

**2.5. X-PEEM Data Analysis.** The C 1s and N 1s reference spectra for PS, PLA, and HSA are plotted in Figure 1. At the C 1s edge, the spectra can be easily differentiated with PS characterized by a C 1s  $\rightarrow \pi^*_{\text{C}=\text{C}}$  transition at 285.15(3) eV. PLA and HSA show strong C 1s  $\rightarrow \pi^*_{\text{C}=\text{O}}$  transitions at 288.53(3) and 288.20(6) eV, respectively. The carbonyl transition in HSA is at a slightly lower energy than that in PLA since the amide functional group (R-CONH) is a less electronegative environment than the ester group (R-COOR').<sup>12</sup> At the N 1s edge,

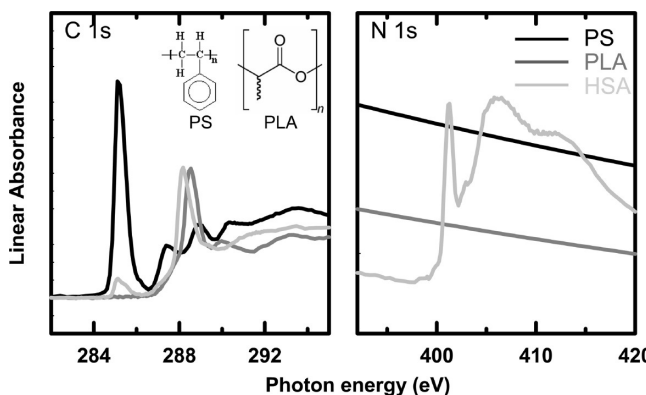


**Figure 1.** C 1s X-ray absorption spectra of PS (black), PLA (dark gray), and HSA (light gray) as recorded in STXM. The spectra are plotted on an absolute linear absorbance scale. In the case of the C 1s signals, linear background was subtracted.

HSA is easily recognized since it is the only component containing nitrogen. PS and PLA are featureless in the N 1s edge.

All data analyses were performed with the aXis2000 software package.<sup>22</sup> C 1s and N 1s image sequences were aligned, if necessary, normalized to the ring current, and divided by the  $I_0$  spectrum collected from a clean, HF-etched Si(111) chip. The  $I_0$  spectrum itself was corrected for the adsorption of the underlying silicon, as well as with a linear energy term representing the bolometric response of the PEEM detection. All carbon stacks were calibrated by assigning the C 1s  $\rightarrow \pi^*_{\text{C}=\text{C}}$  transition of PS to 285.15 eV, while the nitrogen stacks were calibrated at the N 1s  $\rightarrow \pi^*_{\text{amide}}$  transition, which occurs at 401.20(5) eV.<sup>21</sup>

The spectra at each pixel of the C 1s image sequence were fit to PS, PLA, and HSA reference spectra by means of singular value decomposition (SVD), an optimized method for least-squares analysis in highly overdetermined data sets.<sup>23,24</sup> At the N 1s edge, because neither PS nor PLA show any transitions, only the spectra of PS and HSA are used in the fit, with areas strong in PS thus representing both PS and PLA. PS was included in the fit to account for a slightly downward sloping background arising from the C 1s continuum. The fit coefficients generated from the SVD analysis are presented as component maps, which are the spatial distributions of each component. Skewed illumination was corrected by dividing the whole stack with a heavily smoothed version of the sum of all the component maps. Finally, the intensities were adjusted so as to give quantitative results by dividing the intensity of each image in the image sequence by a scale factor, which results in a total average thickness (sum of all components) of 10 nm, the sampling depth of X-PEEM.<sup>21</sup>

For combined C 1s and N 1s chemical mapping, a N 1s stack was collected immediately after a C 1s stack with the same region of interest specifications without further alignment. Only well-aligned stacks were used to avoid further misalignment between the two stacks. Next, both stacks were fit with the reference spectra using the SVD method. The C 1s component images of PS and PLA were combined with the N 1s component map of HSA to yield a more accurate and detailed map of the protein. Although the combination of C 1s and N 1s edges provides a better qualitative analysis of protein localization, we are still investigating the optimization of multiedge fitting for extracting quantitative information. Thus, all quantitative spectral analysis results presented in this paper are those derived from the C 1s edge only.

For quantitative analysis, a threshold mask was applied to each component map to isolate specific pixels corresponding to PS, PLA, or the interface (Figure 2). In this procedure, only pixels above a certain defined value were included. The average NEXAFS spectrum found for each of the three regions was further modified by setting the pre-edge intensity to zero and then fitting the background subtracted spectrum to the PS, PLA, and HSA reference spectra. Several stacks obtained from different regions of the same sample were analyzed as independent repeat measurements, and the results were averaged to

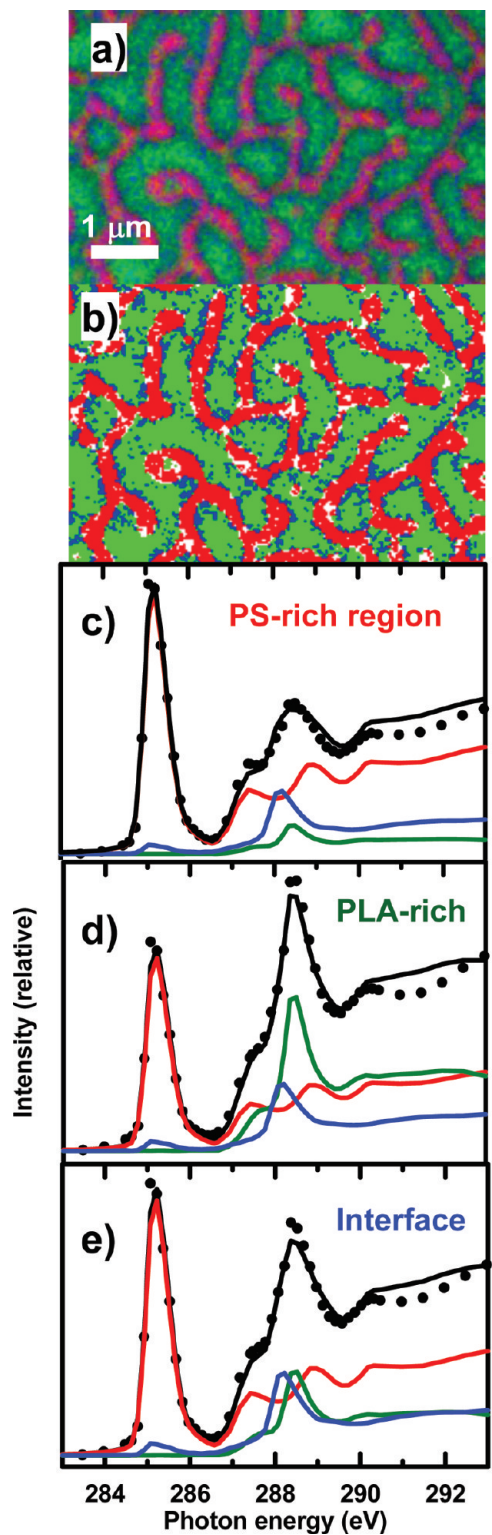


**Figure 2.** (a) Sample X-PEEM color-coded composite map (absolute) derived from SVD analysis, using the PS, PLA, and HSA reference spectra (Figure 1) of a C 1s image sequence (23 energies) recorded from a PS/PLA blend thin film spun-cast from a dichloromethane solution with a total loading of 0.7 wt % polymer in a 40:60 PS/PLA ratio, and annealed 6 h at 45 °C. (b) Mask used to extract spectra of specific regions. Red denotes PS-rich regions, green denotes PLA-rich regions, defined by threshold masking the PS and PLA component maps. The remaining blue pixels define areas at the interface between the PS-rich and PLA-rich domains. (c) Curve fit of the average C 1s spectra of the PS-rich region (data, dots; fit, black line; components, colored lines). (d) Curve fit of the average C 1s spectra of the PLA-rich region (same color coding). (e) Curve fit of the average C 1s spectra of the interface region (same color coding).

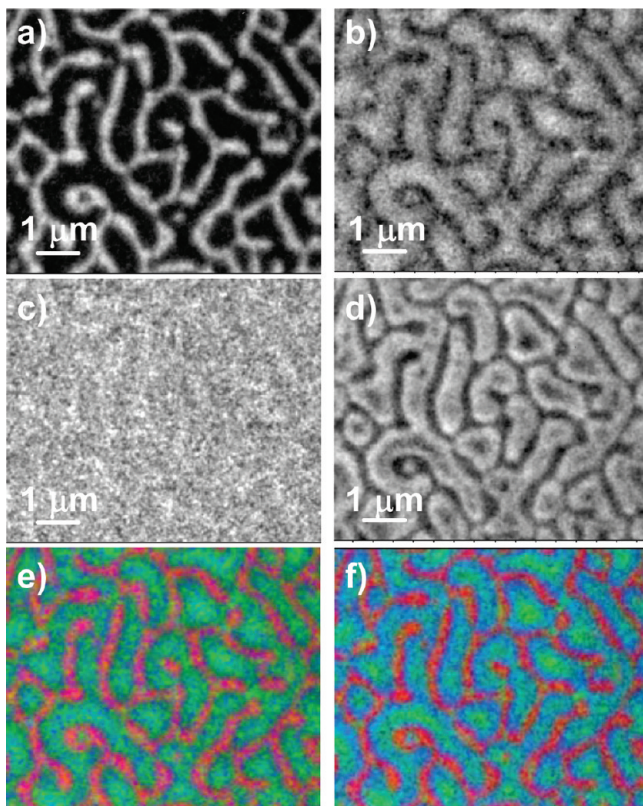


**Figure 3.** Component maps measured from a 40:60 PS/PLA ratio annealed 6 h at 45 °C. Component maps of (a) PS, (b) PLA, (c) HSA, derived from a C 1s image sequence (gray scale is thickness in nm). (d) HSA component map obtained from fit to the N 1s image sequence of the same area. (e) Rescaled color composite map based on component maps derived from the C 1s image sequence (red = PS, green = PLA, blue = HSA). (f) Rescaled color composite map combining maps from C 1s and N 1s (red = PS (C1s), green = PLA (C1s), blue = HSA (N1s)).

obtain the final quantitative values. The uncertainties reported are the standard deviations from these multiple determinations.

**2.6.  $^{125}\text{I}$ -Radiolabeling.** HSA (Sigma Aldrich) was labeled with  $^{125}\text{I}$  (ICN Biomedicals, Mississauga, ON, Canada) using standard radio-iodination methods with IODO-GEN (Pierce Chemical Company, Rockford, IL). The labeled protein was dialyzed overnight against DDI water. Radiolabeling experiments were performed with four repeats by exposing 1 mL solutions of 0.05, 0.01, or 0.005 mg/mL HSA from DDI water or PBS solution for 20 min followed by four static rinses of 2.5 min duration each. Adsorbed amounts were calculated as described earlier.<sup>25</sup>

### 3. Results and Discussion

**3.1. Combined C 1s and N 1s Chemical Mapping.** Figure 3 presents sample component maps obtained from SVD fitting of the reference spectra to representative stacks at the carbon and nitrogen edge of 0.05 mg/mL HSA adsorbed to a PS/PLA 40:60 (0.7 wt %) film annealed for 6 h at 45 °C. At the carbon edge, the use of three reference spectra (PS, PLA, and HSA) in the fit yields three component maps. The bright white pixels of the PS (Figure 3a) and PLA (Figure 3b) maps indicate areas of PS and PLA, respectively. A close examination of the HSA component map (Figure 3c) reveals that the pixels indicative of protein are brightest at the interface between the PS and PLA continuous phases. As previously shown for blood protein adsorption to PS/PMMA films, the interface is the area of lowest free energy and thus the preferred site of adsorption.<sup>12,13</sup>

The nitrogen edge is very sensitive to protein as it is the only nitrogen-containing species in this system. As demonstrated by the protein component map derived from the N 1s sequence (Figure 3d), HSA adsorbs most extensively to the interface between the PS and PLA cocontinuous domains (as determined from the C 1s analysis) but also has significant signal on the PLA-rich domain. This is evident by the dark gray areas corresponding to continuous PS and also a darker area toward the center of the domains corresponding to PLA. The tricolor coded composite component map based only on the C 1s image sequence component maps (Figure 3e) reveals that the protein (color coded in blue) is strongest at the interface between PS (red) and PLA (green). Because the carbon and nitrogen stacks are collected at the exact same region, the component maps of PS and PLA (which are easily distinguishable at the carbon edge) can be combined with the HSA component map from the N 1s edge. The resulting map (Figure 3f) reveals the protein distribution relative to the substrate components with much greater precision than the analysis based solely on the C 1s image sequence. The site of preferential HSA adsorption occurs at the interface between the two polymer domains.

X-PEEM chemical mapping using combined carbon and nitrogen ls edges provides a means for mapping HSA through a combination of near edge and elemental discrimination. Among the available species-specific microscopy techniques, scanning X-ray photoemission microscope (SPEM)<sup>26</sup> has similar capabilities to X-PEEM. However, X-PEEM currently has better spatial resolution (<50 nm) relative to SPEM (~150 nm) and lower radiation damage rates. STXM is a complementary technique to X-PEEM because X-rays transmit through the entire polymer film; however, X-PEEM is more sensitive to adsorbed protein since it probes only the top 10 nm of the film surface. Furthermore, some X-PEEM microscopes such as those at Elettra and the Canadian Light Source (CLS) have energy filters that allow for XPS imaging at slightly better spatial resolution. Electron energy loss spectroscopy (EELS) in transmission electron microscopes (TEM) offers 5 nm (or lower) spatial resolution.<sup>27</sup> However, this technique is very limited for biomaterial applications due to much higher radiation damage<sup>28,29</sup> and poorer energy resolution than X-ray techniques.

**3.2. Effect of Topography.** Previously, the miscibility and morphology of three PS/PLA 40:60 (0.7 wt %) films were examined as a function of annealing times (1 h vs 6 h) and temperatures (45 and 70 °C).<sup>16</sup> It was found that annealing at 45 °C for 1 and 6 h led to a progressive coarsening of the PLA continuous domains, with the height of the domains increasing by 10 nm, as judged by AFM. Annealing at 70 °C for 1 h, in excess of the glass transition temperature ( $T_g$ ) of PLA ( $T_g \sim 60$  °C), resulted in a phase inversion where the discrete domains were composed of PS. The PS domains doubled in height (~90 nm) at this temperature.

Strikingly, although the morphology of the PS-PLA films changed significantly with vacuum annealing, the quantitative results from X-PEEM<sup>16</sup> revealed the composition of the blends to be similar, with the percentages of PS and PLA varying by only 10 and 13% in the PS and PLA regions, respectively, for the three films annealed for 1 h at 45 °C, 6 h at 45 °C, and 1 h at 70 °C. However, the rugosity of these three films varied from 35 to 90 nm (rms fluctuation). Thus, the three films provide chemically similar platforms for protein adsorption studies and allow an investigation of the effect of topography, independent of surface chemistry.

Figure 4a–c illustrates the rescaled X-ray spectromicroscopy color-coded composite maps of the three films obtained after

exposure to 0.05 mg/mL solutions of HSA from DDI water, while Figure 4d–f presents rescaled X-ray spectromicroscopy color-coded composite maps of the three films (different samples of same history) prior to protein adsorption. In comparison to the PS-PLA films prior to protein adsorption, the X-PEEM composite maps after HSA adsorption show a much more blue color arising from the adsorbed protein. The purely red (PS) and green (PLA) regions in the native films are now “pink” and “turquoise”, clearly indicating that HSA has adsorbed to some extent across the entire surface. Similar to the results obtained from HSA adsorption to PS/PMMA films,<sup>13</sup> a thin band of protein (blue) is seen to adsorb preferentially at the interface, which we thus conclude is the area of lowest free energy.

Table 1 summarizes the quantitative analysis of HSA thicknesses on the PS, PLA and interface regions of these films. Comparison of HSA adsorption to the PS, PLA, and interface regions among the three films reveal markedly consistent adsorption thicknesses, with variations less than 0.5 nm, the estimated uncertainty in the measurements. The data analysis quantifies the preferential adsorption to the interface, with a 0.6–0.9 nm greater HSA thickness at the interface than on the PS or PLA regions (Table 1). Furthermore, comparison of the thicknesses of adsorbed HSA between the PS-PLA films and PS-PMMA films shows clear similarities in the location of preferential adsorption and thickness values.<sup>13</sup> Likely, this similarity arises from the chemical similarity of the PS-PLA and PS-PMMA systems, with PLA and PMMA polymers composed of similar functional groups and, thus, the domains having similar hydrophobicities. The quantitative analyses show a trend of slightly increasing adsorbed HSA thickness as the domain height increases. However, the increase is within the limits of uncertainty.

The data obtained (Table 1) show that topographical variation in the 35–90 nm range does not significantly alter HSA adsorption to PS/PLA. Further evidence is seen in the control experiments where 0.05 mg/mL HSA was adsorbed to flat films spun cast from only PS or PLA. Adsorption on both pure substrates showed thickness of adsorbed HSA (1.4(5) nm on pure PS; 1.7(5) nm on pure PLA) similar to that on the blended films.

There are conflicting reports in the literature on the dependence of protein adsorption on topography. Small structures below ~5 nm<sup>30–32</sup> appear to result in a higher amount of adsorbed protein, whereas for some proteins, larger structures (greater than 10 nm) do not affect the adsorbed quantity.<sup>33</sup> It has been postulated that larger structures appear as smooth surfaces for proteins, and the effective surface area is increased by only a small amount.<sup>30</sup> Nonetheless, it is evident that this behavior is highly protein specific. For example, a titanium substrate patterned by local anodic oxidation to exhibit 1–2 nm high or 3–4 nm high titanium lines (fwhm 40 nm) revealed F-actin to preferentially adsorb to the 1–2 nm high structures, while protein A (and subsequently IgG) showed no preference to structures of either height.<sup>31</sup> Also, it was shown that increasing the root-mean-square roughness of evaporated tantalum films from 2 to 40 nm resulted in increased adsorption of fibrinogen and conformational changes in adsorbed fibronectin.<sup>34,35</sup> More relevant to the present work, surface roughness variations in titanium from 2 to 20 nm were reported not to affect the amount of HSA adsorbed.<sup>33</sup> Thus, the observation in the present work that topography had no effect on albumin adsorption to PS-PLA films may be due to the intrinsic nature of HSA itself.

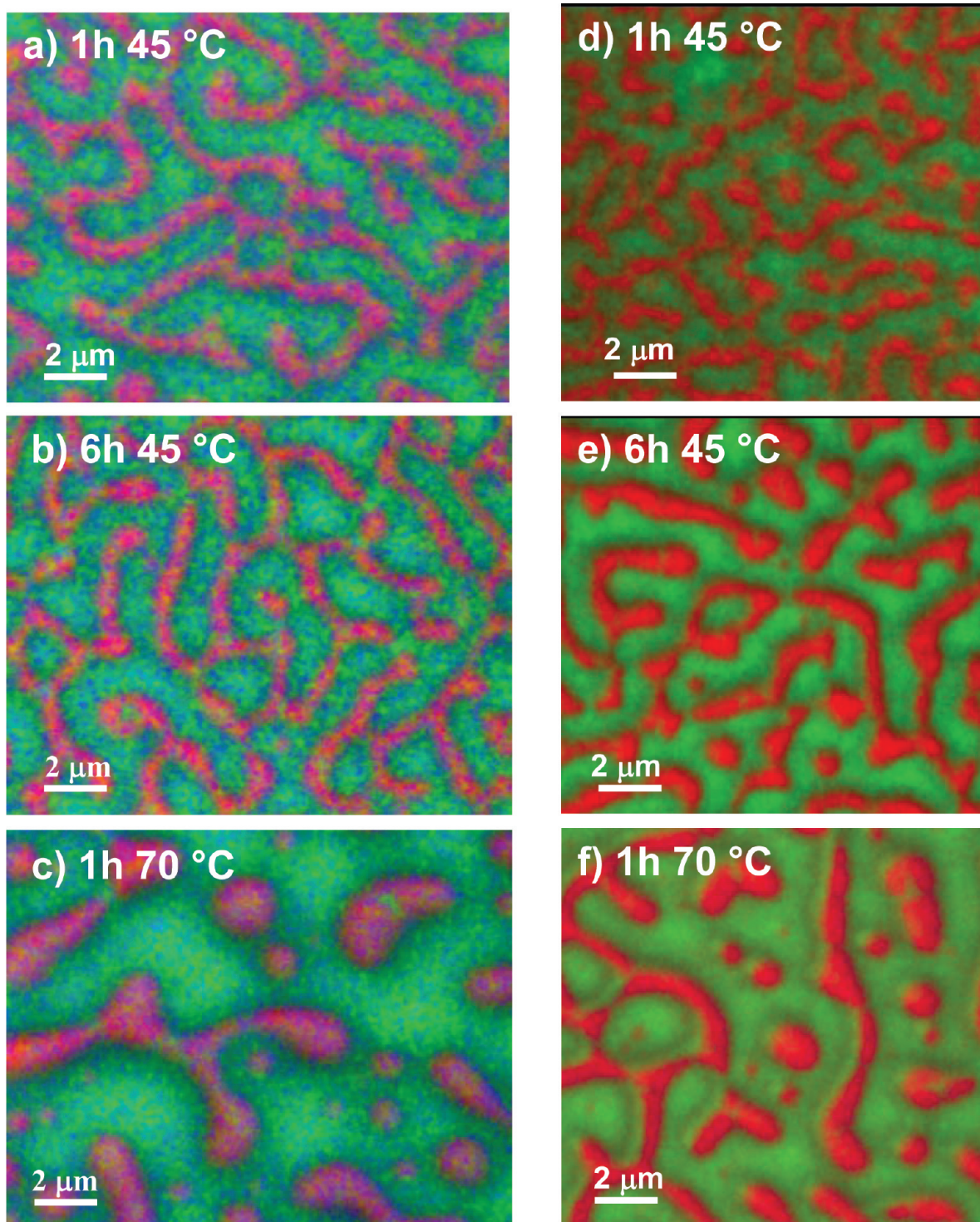


**Figure 4.** (Left) X-PEEM rescaled color-coded composite maps of 40:60 PS/PLA films (0.7 wt % loading) annealed at (a) 1 h at 45 °C, (b) 6 h at 45 °C, (c) 1 h at 70 °C and exposed to 0.05 mg/mL solutions of HSA from DDI water. The maps were derived from C 1s image sequences. PS is coded red, PLA is coded green, and HSA is coded blue. (Right) Color coded maps from C 1s image sequences of PS/PLA spun cast films (without adsorbed protein) vacuum annealed for (d) 1 h at 45 °C, (e) 6 h at 45 °C, (f) 1 h at 70 °C.

**3.2. Effect of Salts.** Three concentrations of HSA (0.005, 0.01, and 0.05 mg/mL) in DDI water and PBS buffer were exposed to the PS/PLA 40:60 (0.7 wt %) film annealed for 1 h at 70 °C. Figure 5a–f and g–l present the color-coded maps obtained for the three films immersed in DDI water and PBS buffer protein solutions, respectively. For the DDI system, the rescaled images reveal that at the highest protein concentration (0.05 mg/mL) HSA (blue) preferentially

adsorbs to the interface between the PS and PLA domains, as evidenced by a thin band of blue. As the protein concentration decreases, the band disappears and the blue color is more evenly spread across the surface. The color composite map presented on an absolute scale for the 0.05 mg/mL system (Figure 5b) shows more turquoise and pink colors suggesting slightly higher protein adsorption, while that for lower concentration (0.005 mg/mL, Figure 5f)

**Table 1.** Thickness (nm) of PS, PLA, and HSA in the PS, PLA, and Interface from PS/PLA 40:60 (0.7 wt %) Films<sup>a</sup>

region	composite thickness (nm)	0.05 mg/mL HSA		
		1 h, 45 °C	6 h, 45 °C	1 h, 70 °C
PS	PS	6.3	7.0	8.1
	PLA	2.1	0.9	0.0
	HSA	1.7	2.1	1.9
PLA	PS	2.7	2.9	2.5
	PLA	5.4	5.2	5.1
	HSA	1.9	1.9	2.4
interface	PS	4.4	4.7	6.5
	PLA	3.3	2.5	0.7
	HSA	2.3	2.8	2.7

<sup>a</sup> Films were annealed 1 h at 45 °C, 6 h at 45 °C, and 1 h at 70 °C. Uncertainty: ±0.5 nm.

exhibits many bright green pixels, implying less uniform distribution of protein.

The rescaled images of the samples in the PBS buffer system (Figure 5g,i,k) demonstrate similar shades of turquoise and pink. The images at the higher concentrations (0.05 and 0.01 mg/mL) reveal preferential protein adsorption to the interface between PS and PLA domains. The blue color of the absolute image of the film exposed to 0.05 mg/mL HSA (from PBS buffer, Figure 5h) is indicative of a high amount of adsorbed protein. As the concentration decreases, the images gain a significantly “greener” and “redder” hue, indicating decreased protein adsorption. Qualitatively, at higher protein concentrations (0.05 mg/mL HSA), HSA shows greater adsorption from a PBS compared to a DDI solution; however, at lower concentrations (0.01 and 0.005 mg/mL HSA), similar thicknesses of adsorbed protein are observed in both systems.

The quantitative results obtained from the spectral fitting for the films exposed to protein from DDI water reveal that, regardless of concentration, protein adsorption is the most extensive at the interface between PS and PLA (Table 2). As the concentration of HSA decreases, the average thickness of protein across the entire polymer surface also decreases. Comparison of adsorption on PS and PLA regions at a particular concentration shows a slight preference for the PS region, similar to the PS/PMMA system.<sup>13,14</sup> This similarity may be due to the presence of the ester functional group in both PLA and PMMA.

The quantitative results for HSA adsorption from PBS buffer also show preferential adsorption at the interface; however, the thickness values are almost twice as great as those detected in DDI water at the interface for all three protein concentrations. The X-PEEM results reveal a general increase in the thickness of adsorbed protein with increasing ionic strength (especially on the PLA and interface regions), which appears to conflict with literature reports showing a decrease in adsorbed quantity with increasing salt concentration on silica, pegylated Nb<sub>2</sub>O<sub>5</sub>, and Si(Ti)O<sub>2</sub> surfaces, as determined using neutron reflectivity,<sup>36</sup> optical waveguide light mode spectroscopy,<sup>37</sup> and integrated optical methods,<sup>38</sup> respectively. However, according to the latter studies, although the number of protein molecules decreased with increasing ionic strength, the area occupied by the adsorbed molecules increased almost 10-fold at a NaCl concentration of 0.5 mol/L.<sup>38</sup>

The increased HSA thickness detected for adsorption from buffer, especially in the PLA and interface regions, could be due to an increased number of adsorbed HSA molecules or to a change in conformation resulting in increasing size, with no change in the number density. To investigate these possibilities, adsorbed quantities were measured using <sup>125</sup>I-labeled HSA under

## Rescaled      Absolute

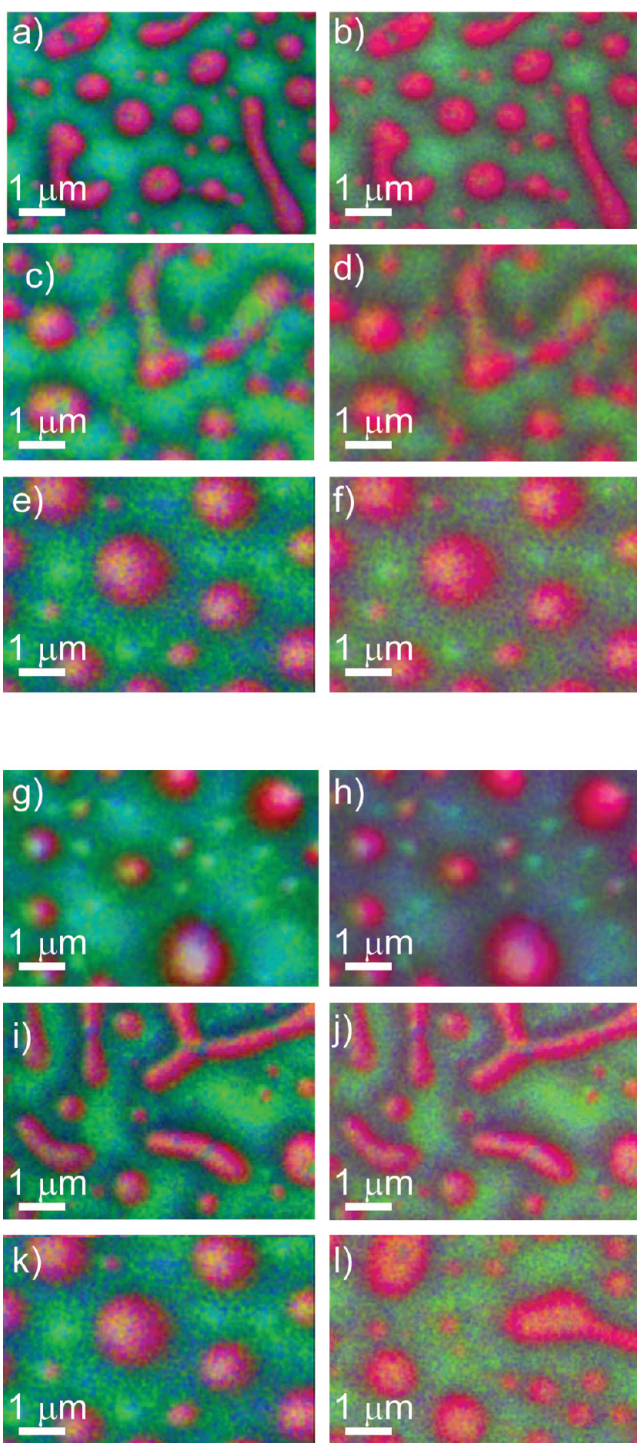


**Figure 5.** X-PEEM color coded composite maps of 40:60 PS/PLA films (0.7 wt % loading), annealed 1 h at 70 °C with protein adsorbed from DDI water: (a) 0.05 mg/mL HSA (rescaled), (b) 0.05 mg/mL HSA (absolute), (c) 0.01 mg/mL HSA (rescaled), (d) 0.01 mg/mL HSA (absolute), (e) 0.005 mg/mL HSA (rescaled), and (f) 0.005 mg/mL HSA (absolute). Same polymer composition with protein adsorbed from PBS buffer: (g) 0.05 mg/mL HSA (rescaled), (h) 0.05 mg/mL HSA (absolute), (i) 0.01 mg/mL HSA (rescaled), (j) 0.01 mg/mL HSA (absolute), (k) 0.005 mg/mL HSA (rescaled), (l) 0.005 mg/mL HSA (absolute). PS is coded red, PLA is coded green, and HSA is coded blue.

identical conditions from both DDI and PBS solution (Figure 6). The radiolabeling method provides a means of measuring

**Table 2.** Thickness (nm) of PS, PLA, and HSA in the PS, PLA, and Interface Regions from PS/PLA 40:60 (0.7 wt %) Films<sup>a</sup>

region	composite thickness (nm)	HSA adsorbed from DDI			HSA adsorbed from PBS		
		0.05 mg/mL	0.01 mg/mL	0.005 mg/mL	0.05 mg/mL	0.01 mg/mL	0.005 mg/mL
PS	PS	8.1	8.0	9.0	7.8	8.3	9.2
	PLA	0.0	0.9	0.2	0.2	0.3	0.2
	HSA	1.9	1.1	0.8	2.0	1.4	0.7
PLA	PS	2.5	3.0	3.0	2.6	2.5	2.7
	PLA	5.1	6.1	6.7	4.7	6.0	6.5
	HSA	2.4	0.9	0.3	2.8	1.5	0.8
interface	PS	6.5	5.1	3.8	3.9	4.6	4.6
	PLA	0.7	3.1	4.5	2.0	2.5	2.7
	HSA	2.7	1.8	1.7	4.1	3.5	2.8

<sup>a</sup> Films annealed 1 h at 70 °C and exposed to 0.05, 0.01, and 0.005 mg/mL HSA from either DDI water or PBS buffer. Uncertainty: ±0.5 nm.

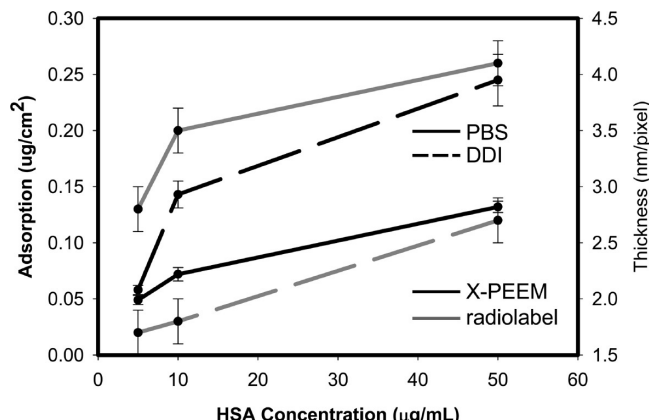


**Figure 6.** Isotherms for adsorption of <sup>125</sup>I-labeled HSA from PBS and DDI water. PBS is solid and DDI is dashed. X-PEEM detected thickness is plotted in gray, radiolabeling in black.

**Table 3.** <sup>125</sup>I Radiolabeling Experiments<sup>a</sup>

concentration	DDI	sd	PBS	sd
0.005	0.058	0.004	0.049	0.004
0.01	0.143	0.012	0.072	0.006
0.05	0.245	0.023	0.132	0.005

<sup>a</sup> HSA adsorption ( $\mu\text{g}/\text{cm}^2$ ) from DDI water or PBS buffer with standard deviations (sd,  $n = 4$ ).

the number of adsorbed protein molecules, independent of their conformation. The data from these experiments showed that at the higher concentrations (0.05 and 0.01 mg/mL protein) the number of HSA molecules adsorbed from DDI water is almost double that from buffer, while similar numbers of molecules were adsorbed from both media at the lowest concentration (0.005 mg/mL HSA; Table 3). These results are in striking contrast to the X-PEEM data, which showed increasing thicknesses of HSA on the PLA and interface regions with increasing ionic strength. Thus, we conclude that if the number of adsorbed protein molecules is lower for adsorption from PBS compared to DDI water (as judged by radiolabeling) then the increased thickness detected from X-PEEM must arise from a change in conformation to a more extended structure.

In the case of charged surfaces, previous studies<sup>36–38</sup> have attributed the decrease in protein adsorption at higher ionic strength to electrostatic effects. Here we show that such a decrease occurs on a neutral substrate. We speculate that in DDI water, the hydrophilic, charged amino acid residues of HSA are likely less exposed compared to PBS buffer; thus, water molecules have an increased opportunity to hydrogen bond (or form structured water) to the more hydrophobic protein molecule in DDI water. When adsorption occurs from this situation (DDI water) there is a greater entropy loss compared to adsorption from PBS buffer where there is a lower extent of entropy loss

since there is less disruption of structured water. Thus, we conclude that the hydrophobic effect plays an important role in protein adsorption to the blend materials studied in this work.

The difference in thicknesses of HSA adsorbed from PBS versus DDI solutions probably arise from changes in protein conformation in solution with change in ionic strength, revealed via comparison of the X-PEEM and radiolabeling results. Therefore, in combination with techniques such as radiolabeling or other methods that measure adsorbed quantity, X-PEEM provides an effective, albeit indirect, approach to probing conformational changes in adsorbed protein that may give rise to a change in thickness.

#### 4. Conclusions

The adsorption of HSA to PS-PLA surfaces was studied by X-PEEM and radiolabeling. The influence of topography, buffer conditions, and annealing on the adsorption were investigated. No significant changes in adsorption were observed upon increasing the surface roughness of the substrate. By investigating the adsorption of HSA from PBS and DDI water solutions and comparing the results of X-PEEM and radiolabeling experiments, it is concluded tentatively that the HSA molecule is expanded in PBS compared to DDI water.

**Acknowledgment.** This research is supported by the Natural Sciences and Engineering Research Council of Canada (NSERC), AFMNet, and the Canada Research Chair programs. X-ray microscopy was carried out using PEEM2 and STXM532 at the ALS. The ALS is supported by the U.S. Department of Energy under Contract DE-AC03-76SF00098.

#### References and Notes

- Saravanan, M.; Bhaskar, K.; Srinivasa, R. G.; Dhanaraju, M. D. *J. Microencapsulation* **2003**, *20*, 289–302.
- Cai, Q.; Bei, J.; Wang, S. *Polym. Adv. Technol.* **2002**, *13*, 534–540.
- Biresaw, G.; Carriere, C. J.; Willett, J. L. *J. Appl. Polym. Sci.* **2004**, *94*, 65–73.
- Zhang, G.; Zhang, J.; Wang, S.; Shen, D. *J. Polym. Sci., Part B: Polym. Phys.* **2003**, *41*, 23–30.
- Castner, D. G.; Ratner, B. D. *Surf. Sci.* **2002**, *500*, 28–60.
- Yasugi, K.; Nagasaki, Y.; Kato, M.; Kataoka, K. *J. Controlled Release* **1999**, *62*, 89–100.
- Agrawal, S. K.; Sanabria-DeLong, N.; Coburn, J. M.; Tew, G. N.; Bhatia, S. R. *J. Controlled Release* **2006**, *112*, 64–71.
- Zhou, S.; Liao, X.; Li, X.; Deng, X.; Li, H. *J. Controlled Release* **2003**, *86*, 195–205.
- Jeong, J. H.; Lim, D. W.; Han, D. K.; Park, T. G. *Colloids Surf., B* **2000**, *18*, 371–379.
- Vittaz, M.; Bazile, D.; Spenlehauer, G.; Verrecchia, T.; Veillard, M.; Puisieux, F.; Labarre, D. *Biomaterials* **1996**, *17*, 1575–1561.
- Lucke, A.; Tebmar, J.; Schnell, E.; Schmeer, G.; Gopferich, A. *Biomaterials* **2000**, *21*, 2361–2370.

- (12) Morin, C.; Hitchcock, A. P.; Cornelius, R. M.; Brash, J. L.; Scholl, A.; Doran, A. *J. Electron. Spectrosc. Relat. Phenom.* **2004**, *137*–140, 785–794.
- (13) Li, L.; Hitchcock, A. P.; Robar, N.; Cornelius, R.; Brash, J. L.; Scholl, A.; Doran, A. *J. Phys. Chem. B* **2006**, *110*, 16763–16773.
- (14) Li, L.; Hitchcock, A. P.; Cornelius, R.; Brash, J. L.; Scholl, A.; Doran, A. *J. Phys. Chem. B* **2008**, *112*, 2150–2158.
- (15) Leung, B. O.; Hitchcock, A. P.; Brash, J. L.; Scholl, A.; Doran, A.; Henklein, P.; Overhage, J.; Hilpert, K.; Hale, J. D.; Hancock, R. E. W. *Biointerphases* **2008**, *3*, F27–F35.
- (16) Leung, B. O.; Hitchcock, A. P.; Brash, J. L.; Scholl, A.; Doran, A. *Macromolecules* **2009**, *42*, 1679–1684.
- (17) Warwick, T.; Ade, H.; Kilcoyne, A. L. D.; Kritscher, M.; Tyliszczak, T.; Fakra, S.; Hitchcock, A. P.; Hitchcock, P.; Padmore, H. A. *J. Synchrotron Radiat.* **2002**, *9*, 254–257.
- (18) Kilcoyne, A. L. D.; Tyliszczak, T.; Steele, W. F.; Fakra, S.; Hitchcock, P.; Franck, K.; Anderson, E.; Harteneck, B.; Rightor, E. G.; Mitchell, G. E.; Hitchcock, A. P.; Yang, L.; Warwick, T.; Ade, H. *J. Synchrotron Radiat.* **2003**, *10*, 125–136.
- (19) Jacobsen, C. J.; Zimba, C.; Flynn, G.; Wirick, S. *J. Microsc. (Oxford, U.K.)* **2000**, *197*, 173–184.
- (20) Anders, S.; Padmore, H. A.; Duarte, R. M.; Renner, T.; Stammier, T.; Scholl, A.; Scheinein, M. R.; Stohr, J.; Seve, L.; Sinkovic, B. *Rev. Sci. Instrum.* **1999**, *70*, 3973–3981.
- (21) Wang, J.; Li, L.; Morin, C.; Hitchcock, A. P.; Doran, A.; Scholl, A. *J. Electron Spectrosc. Relat. Phenom.* **2009**, *170*, 25–36.
- (22) aXis2000 is free for noncommercial use. It is written in Interactive Data Language (IDL) and available from <http://unicorn.mcmaster.ca/axis2000.html>.
- (23) Strang, G. In *Linear Algebra and Its Applications*; Harcourt Brace Jovanovich: San Diego, CA, 1988.
- (24) Koprinarov, I. N.; Hitchcock, A. P.; McCrory, C. T.; Childs, R. F. *J. Phys. Chem. B* **2002**, *106*, 5358–5364.
- (25) Chan, B. M. C.; Brash, J. L. *J. Colloid Interface Sci.* **1981**, *82*, 217–225.
- (26) Goldoni, A.; Larciprete, R.; Gregoratti, L.; Kaulich, B.; Kiskinova, M.; Zhang, Y.; Dai, H.; Sangalli, L.; Parmigiani, F. *App. Phys. Lett.* **2002**, *80*, 2165–2167.
- (27) Sugena, K.; Tence, M.; Mory, C.; Colliex, C.; Kato, H.; Okazaki, T.; Shinohara, H.; Hirahara, K.; Bandow, S.; Iijima, S. *Science* **2000**, *290*, 2280–2282.
- (28) Rightor, E. G.; Hitchcock, A. P.; Ade, H.; Leapman, R. D.; Urquhart, S. G.; Smith, A. P.; Mitchell, G.; Fischer, D.; Shin, H. J.; Warwick, T. *J. Phys. Chem. B* **1997**, *101*, 1950–1960.
- (29) Wang, J.; Botton, G. A.; West, M. M.; Hitchcock, A. P. *J. Phys. Chem. B* **2009**, *113*, 1869–1876.
- (30) Macarena Blanco, E.; Horton, M. A.; Mesquida, P. *Langmuir* **2008**, *24*, 2284–2287.
- (31) Gallia, C.; Collaud Coen, M.; Hauert, R.; Katanaev, V. L.; Gröning, P.; Schlapbach, L. *Colloids Surf., B* **2002**, *26*, 255–267.
- (32) Dolatshahi-Pirouz, A.; Rechendorff, K.; Hovgaard, M. B.; Foss, M.; Chevallier, J.; Besenbacher, F. *Colloids Surf., B* **2008**, *66*, 53–59.
- (33) Cai, K.; Bossert, J.; Jandt, K. D. *Colloids Surf., B* **2006**, *49*, 136–144.
- (34) Rechendorff, K.; Hovgaard, M. B.; Foss, M.; Zhdanov, V. P.; Besenbacher, F. *Langmuir* **2006**, *22*, 10885–10888.
- (35) Hovgaard, M. B.; Rechendorff, K.; Chevallier, J.; Foss, M.; Besenbacher, F. *J. Phys. Chem. B* **2008**, *112*, 8241–8249.
- (36) Su, T. J.; Lu, J. R.; Thomas, R. K.; Cui, Z. F.; Penfold, J. *J. Colloids Interface Sci.* **1998**, *203*, 419–429.
- (37) Pache, S.; Voros, J.; Griesser, H. J.; Spencer, N. D.; Textor, M. *J. Phys. Chem. B* **2008**, *109*, 17545–17552.
- (38) Ramsden, J. J.; Prensil, J. E. *J. Phys. Chem.* **1994**, *98*, 5376–5381.

BM900264W